Progress In Electromagnetics Research B, Vol. 26, 115–147, 2010

HELICAL WAVEGUIDE WITH TWO BENDINGS, AND APPLICATIONS

Z. Menachem and S. Tapuchi

Department of Electrical Engineering
Sami Shamoon College of Engineering
Israel

Abstract—This paper presents an improved approach for the propagation of electromagnetic (EM) fields along a helical hollow waveguide that consists of two bendings in the same direction. In this case, the objective is to develop a mode model for infrared (IR) wave propagation, in order to represent the effect of the radius of the cylinder of the helix and the step's angle on the output fields and the output power transmission. This model enables us to understand more precisely the influence of the step's angle and the radius of the cylinder of the helix on the output results of each section (bending). The output transverse components of the field, the output power transmission and the output power density for all bending are improved by increasing the step's angle or the radius of the cylinder of the helix, especially in the cases of space curved waveguides. This mode model can be a useful tool to improve the output results in all the cases of the helical hollow waveguides with two bendings for industrial and medical regimes.

1. INTRODUCTION

Various methods of cylindrical hollow metallic or metallic with inner dielectric coating waveguide have been proposed in the literature [1–18]. A review of the hollow waveguide technology [1, 2] and a review of IR transmitting, hollow waveguides, fibers and integrated optics [3] were published. The first theoretical analysis of the problem of hollow cylindrical bent waveguides was published by Marcatili and Schmeltzer [4], where the theory considers the bending as a small disturbance and uses cylindrical coordinates to solve Maxwell

Received 15 August 2010, Accepted 19 September 2010, Scheduled 29 September 2010
Corresponding author: Z. Menachem (zionm@post.tau.ac.il).

equations. They derive the mode equations of the disturbed waveguide using the ratio of the inner radius r to the curvature radius R as a small parameter ($r/R \ll 1$). Their theory predicts that the bending has little influence on the attenuation of a hollow metallic waveguide. However, practical experiments have shown a large increase in the attenuation, even for a rather large R.

Marhic [5] proposed a mode-coupling analysis of the bending losses of circular metallic waveguide in the IR range for large bending radii. In the circular guide it is found that the preferred TE_{01} mode can couple very effectively to the lossier TM_{11} mode when the guide undergoes a circular bend. The mode-coupling analysis [5] developed to study bending losses in microwave guides has been applied to IR metallic waveguides at $\lambda = 10.6\,\mu\text{m}$. For circular waveguides, the microwave approximation has been used for the index of refraction and the straight guide losses, and the results indicate very poor bending properties due to the near degeneracy of the TE_{01} and TM_{11} modes, thereby offering an explanation for the high losses observed in practice.

Miyagi et al. [6] suggested an improved solution, which provided agreement with the experimental results, but only for $r/R \ll 1$. A different approach [5, 7] treats the bending as a perturbation that couples the modes of a straight waveguide. That theory explains the large difference between the metallic and metallic-dielectric bent waveguide attenuation. The reason for this difference is that in metallic waveguides the coupling between the TE and TM modes caused by the bending mixes modes with very low attenuation and modes with very high attenuation, whereas in metallic-dielectric waveguides, both the TE and TM modes have low attenuation. The EH and HE modes have similar properties and can be related to modes that have a large TM component.

Hollow waveguides with both metallic and dielectric internal layers were proposed to reduce the transmission losses. Hollow-core waveguides have two possibilities. The inner core materials have refractive indices greater than one (namely, leaky waveguides) or the inner wall material has a refractive index of less than one. A hollow waveguide can be made, in principle, from any flexible or rigid tube (plastic, glass, metal, etc.) if its inner hollow surface (the core) is covered by a metallic layer and a dielectric overlayer. This layer structure enables us to transmit both the TE and TM polarization with low attenuation [5, 7].

A method for the EM analysis of bent waveguides [8] is based on the expansion of the bend mode in modes of the straight waveguides, including the modes under the cutoff. A different approach to calculate the bending losses in curved dielectric waveguides [9] is based on

the well-known conformal transformation of the index profile and on vectorial eigenmode expansion combined with perfectly matched layer boundary conditions to accurately model radiation losses. An improved ray model for simulating the transmission of laser radiation through a metallic or metallic dielectric multibent hollow cylindrical waveguide was proposed in [10, 11]. It was shown theoretically and proved experimentally that the transmission of CO_2 laser radiation is possible even through bent waveguide.

The propagation of EM waves in a loss-free inhomogeneous hollow conducting waveguide with a circular cross section and uniform plane curvature of the longitudinal axis was considered in [12]. For small curvature the field equations can be solved by means of an analytical approximation method. In this approximation the curvature of the axis of the waveguide was considered as a disturbance of the straight circular cylinder, and the perturbed torus field was expanded in eigenfunctions of the unperturbed problem. An extensive survey of the related literature can be found especially in the book on EM waves and curved structures [13]. The radiation from curved open structures is mainly considered by using a perturbation approach, that is by treating the curvature as a small perturbation of the straight configuration. The perturbative approach is not entirely suitable for the analysis of relatively sharp bends, such as those required in integrated optics and especially short millimeter waves.

The models based on the perturbation theory consider the bending as a perturbation ($r/R \ll 1$), and solve problems only for a large radius of curvature.

Several methods of propagation along the toroidal and helical waveguides were developed in [14–18], where the derivation is based on Maxwell's equations. The method in [14] has been derived for the analysis of EM wave propagation in dielectric waveguides with arbitrary profiles, with rectangular metal tubes, and along a curved dielectric waveguide. An improved approach has been derived for the propagation of EM field along a toroidal dielectric waveguide with a circular cross-section [15]. The method in [16] has been derived for the propagation of EM field along a helical dielectric waveguide with a circular cross section. The method in [17] has been derived for the propagation of EM field along a helical dielectric waveguide with a rectangular cross section. It is very interesting to compare between the mode model methods for wave propagation in the waveguide with a rectangular cross section, as proposed in Refs. [14, 17] as regard to the mode model methods for wave propagation in the waveguide with a circular cross section, as proposed in [15, 16]. The methods in [14, 15] have been derived for one bending of the toroidal waveguide

(approximately a plane curve) in the case of small values of step angle of the helix. The methods in [16, 17] have been derived for one bending of the helical waveguide (a space curved waveguide) for an arbitrary value of the step's angle of the helix. The method in [18] has been derived for the propagation of EM field along the toroidal waveguide that consists of two bendings in the same direction, and the main steps of the method for the two bendings were introduced, in detail, for small values of step angles. The methods in [14–18] employ toroidal or helical coordinates (and not cylindrical coordinates, such as in the methods that considered the bending as a perturbation ($r/R \ll 1$)).

The calculations in all the two above methods [14–18], are based on using Laplace and Fourier transforms, and the output fields are computed by the inverse Laplace and Fourier transforms. Laplace transform on the differential wave equations is needed to obtain the wave equations (and thus also the output fields) that are expressed directly as functions of the transmitted fields at the entrance of the waveguide at $\zeta = 0^+$. Thus, the Laplace transform is necessary to obtain the comfortable and simple *input-output* connections of the fields. The objective in all these methods [14–18] was to develop a mode model in order to provide a numerical tool for the calculation of the output fields for a curved waveguide. The technique of the methods is quite different. The technique for a rectangular cross section [14, 17] is based on Fourier coefficients of the transverse dielectric profile and those of the input wave profile, and the output fields were computed by the inverse Laplace and Fourier transforms. On the other hand, the technique for a circular cross section [15, 16, 18] was based on the development of the longitudinal components of the fields into Fourier-Bessel series, and the transverse components of the fields were expressed as functions of the longitudinal components in the Laplace plane and were obtained by using the inverse Laplace transform.

The main objective of this paper is to generalize the method [18] from a toroidal dielectric waveguide (approximately a plane curve) with two bendings to a helical waveguide (a space curved waveguide for an arbitrary value of the step's angle of the helix) with two bendings. The objective is to presents an improved approach for the propagation of EM field in the case of the helical waveguide that consists of two bendings in the same direction. The main steps of the method for the helical waveguide with two bendings will be introduced in the derivation, for arbitrary values of the step's angle (and not for small values of step angles). Our method employs helical coordinates (and not cylindrical coordinates, such as in the methods that considered the bending as a perturbation ($r/R \ll 1$)). The derivation for the first section and the second section of the helical waveguide with the two

bendings is based on Maxwell's equations. The separation of variables is obtained by using the orthogonal-relations. The longitudinal components of the fields are developed into the Fourier-Bessel series. The transverse components of the fields are expressed as functions of the longitudinal components in the Laplace plane and are obtained by using the inverse Laplace transform by the residue method. The results of this model are applied to the study of helical hollow waveguides with two bendings, that are suitable for transmitting IR radiation, especially CO_2 laser radiation. In this paper, we supposed that the modes excited at the input of the waveguide by the conventional CO_2 laser IR radiation ($\lambda = 10.6\,\mu m$) are closer to the TEM polarization of the laser radiation. The TEM_{00} mode is the fundamental and the most important mode. This means that a cross-section of the beam has a Gaussian intensity distribution.

2. THE DERIVATION

The method presented in [18] is generalized from a toroidal waveguide (approximately a plane curve) with two bendings to a helical waveguide (a space curved waveguide for an arbitrary value of the step's angle of the helix) with two bendings. Namely, the calculations in our method are dependent also on the arbitrary value of the step's angle of the helix. This model enables us to understand more precisely the influence of the step's angle and the radius of the cylinder of the helix on the output results of each section (bending).

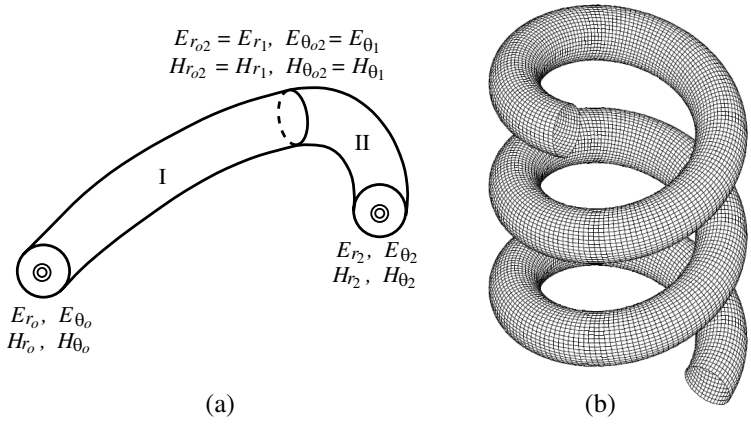

Figure 1. (a) A general scheme for a helical waveguide with two bendings in the same direction. (b) The helical circular waveguide.

Let us assume that the helical waveguide consists of two bendings in the same direction as shown in Fig. 1(a). The helical circular waveguide is shown in Fig. 1(b). The main steps for calculations of the output fields and the output power transmission in the case of the helical waveguide with two bendings in the same direction are introduced in this derivation, based on the method presented in [18]. The coordinates of an arbitrary point on the toroidal system (r, θ, ζ) with a given bending (R) are shown in Fig. 2, where $X = R\cos\phi$ and $Y = R\sin\phi$.

Further, we assume that the first bending (Fig. 1(a)) is R_1, the length is $\zeta_1 = (R_1\phi_1)/\cos\delta_p$, and the metric coefficient is $h_{\zeta_1} = 1 + (r/R_1)\sin\theta\cos^2(\delta_p)$, where δ_p is the step's angle of the helix. Likewise, the radius of the curvature of the second bending is R_2, the length is $\zeta_2 = (R_2\phi_2)/\cos\delta_p$, and the metric coefficient is $h_{\zeta_2} = 1 + (r/R_2)\sin\theta\cos^2(\delta_p)$, as shown in Fig. 1(a). The total length in this case is given by $\zeta = \zeta_1 + \zeta_2$. The cases for a straight waveguide are obtained by letting $R_1 \to \infty$ and $R_2 \to \infty$.

We start by finding the metric coefficients from the helical transformation of the coordinates. The helical transformation of the coordinates is achieved by two rotations and one translation, and is

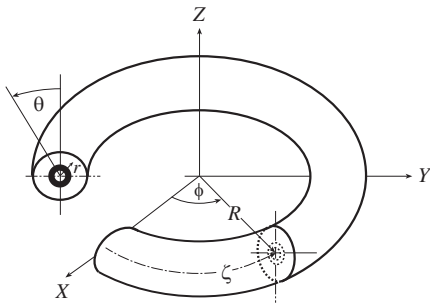

Figure 2. A general scheme of the toroidal system (r, θ, ζ) and the curved waveguide.

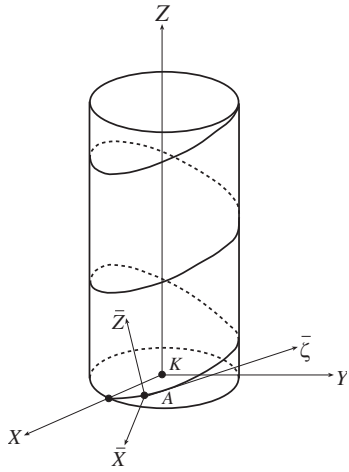

Figure 3. Rotations and translation of the orthogonal system ($\bar{X}$, $\bar{\zeta}$, $\bar{Z}$) from point A to the orthogonal system (X, Y, Z) at point K.

given in the form:

$$\begin{pmatrix} X \\ Y \\ Z \end{pmatrix} = \begin{pmatrix} \cos(\phi_c) & -\sin(\phi_c) & 0 \\ \sin(\phi_c) & \cos(\phi_c) & 0 \\ 0 & 0 & 1 \end{pmatrix} \begin{pmatrix} 1 & 0 & 0 \\ 0 & \cos(\delta_p) & -\sin(\delta_p) \\ 0 & \sin(\delta_p) & \cos(\delta_p) \end{pmatrix} \begin{pmatrix} r & \sin\theta \\ 0 \\ r & \cos\theta \end{pmatrix} + \begin{pmatrix} R\cos(\phi_c) \\ R\sin(\phi_c) \\ \zeta\sin(\delta_p) \end{pmatrix}, \quad (1)$$

where ζ is the coordinate along the helix axis, R is the radius of the cylinder, δ_p is the step's angle of the helix (see Figs. 3–4(a)), and $\phi_c = (\zeta\cos(\delta_p))/R$. Likewise, $0 \leq r \leq a + \delta_m$, where $2a$ is the internal diameter of the cross-section of the helical waveguide, δ_m is the thickness of the metallic layer, and d is the thickness of the dielectric layer (see Fig. 4(b)).

Figure 3 shows the rotations and translation of the orthogonal system $(\bar{X}, \bar{\zeta}, \bar{Z})$ from point A to the orthogonal system (X, Y, Z) at point K. In the first rotation, the $\bar{\zeta}$ and $\bar{Z}$ axes rotate around the $\bar{X}$ axis of the orthogonal system $(\bar{X}, \bar{\zeta}, \bar{Z})$ at the point A until the $\bar{Z}$ axis becomes parallel to the Z axis $(\bar{Z} \parallel Z)$, and the $\bar{\zeta}$ axis becomes parallel to the X, Y plane $(\bar{\zeta} \parallel (X, Y))$ of the orthogonal system (X, Y, Z) at the point K. In the second rotation, the $\bar{X}$ and $\bar{\zeta}$ axes rotate around the $\bar{Z}$ axis $(\bar{Z} \parallel Z)$ of the orthogonal system $(\bar{X}, \bar{\zeta}, \bar{Z})$ until $\bar{X} \parallel X$ and $\bar{\zeta} \parallel Y$. After the two above rotations, we have one translation from the orthogonal system $(\bar{X}, \bar{\zeta}, \bar{Z})$ at the point A to the orthogonal system (X, Y, Z) at the point K.

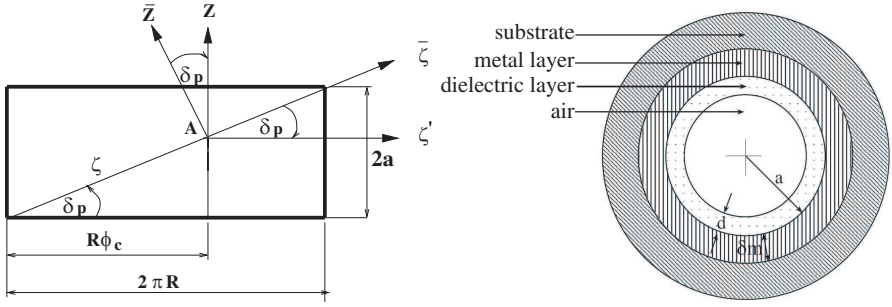

(a) (b)

Figure 4. (a) Deployment of the helix. (b) A cross-section of the waveguide (r, θ).

Figure 4(a) shows the deployment of the helix depicted in Fig. 3. The condition for the step's angle δ_p is given according to

$$\tan(\delta_p) \geq \frac{2(a+\delta_m)}{2\pi R}, \tag{2}$$

where the internal diameter is denoted as $2a$, the thickness of the metallic layer is denoted as δ_m, and the radius of the cylinder is denoted as R.

According to Equation (1), the helical transformation of the coordinates becomes

$$X = (R + r\sin\theta)\cos(\phi_c) + r\sin(\delta_p)\cos\theta\sin(\phi_c), \tag{3a}$$

$$Y = (R + r\sin\theta)\sin(\phi_c) - r\sin(\delta_p)\cos\theta\cos(\phi_c), \tag{3b}$$

$$Z = r\cos\theta\cos(\delta_p) + \zeta\sin(\delta_p). \tag{3c}$$

where $\phi_c = (\zeta/R)\cos(\delta_p)$, R is the radius of the cylinder, and (r, θ) are the parameters of the cross-section. Note that $\zeta\sin(\delta_p) = R\phi_c\tan(\delta_p)$.

The metric coefficients in the case of the helical waveguide according to Equations (3a)–(3c) are:

$$h_r = 1, \tag{4a}$$

$$h_\theta = r, \tag{4b}$$

$$h_\zeta = \sqrt{\left(1+\frac{r}{R}\sin\theta\right)^2\cos^2(\delta_p) + \sin^2(\delta_p)\left(1+\frac{r^2}{R^2}\cos^2\theta\cos^2(\delta_p)\right)}$$

$$= \sqrt{1+\frac{2r}{R}\sin\theta\cos^2(\delta_p)+\frac{r^2}{R^2}\sin^2\theta\cos^2(\delta_p)+\frac{r^2}{R^2}\cos^2\theta\cos^2(\delta_p)\sin^2(\delta_p)}$$

$$\simeq 1+\frac{r}{R}\sin\theta\cos^2(\delta_p). \tag{4c}$$

Furthermore, the third and the fourth terms in the root of the metric coefficient h_ζ are negligible in comparison to the first and the second terms when $(r/R)^2 \ll 1$. Nonetheless, the metric coefficient h_ζ still depends on δ_p, the step's angle of the helix (Fig. 4(a)). Note that the metric coefficient h_ζ is a function of r and θ, which causes a difficulty in the separation of variables. Thus, the analytical methods are not suitable for the helical or the curved waveguide. In this method, the separation of variables is performed by employing the orthogonal-relations. The cross-section of the helical waveguide in the region $0 \leq r \leq a + \delta_m$ is shown in Fig. 4(b), where δ_m is the thickness of the metallic layer, and d is the thickness of the dielectric layer.

Further, we assume that the derivation is based on an arbitrary value of the step's angle of the helix (δ_p). For small values of the step's angle, the helical waveguide becomes a toroidal waveguide, where the

radius of the curvature of the helix can then be approximated by the radius of the cylinder (R). In this case, the toroidal system (r, θ, ζ) in conjunction with the curved waveguide is shown in Fig. 2, and the transformation of the coordinates (3(a)–(c)) is given as a special case of the toroidal transformation of the coordinates, as follows

$$X = (R + r\sin\theta)\cos\left(\frac{\zeta}{R}\right), \tag{5a}$$

$$Y = (R + r\sin\theta)\sin\left(\frac{\zeta}{R}\right), \tag{5b}$$

$$Z = r\cos\theta, \tag{5c}$$

and the metric coefficients are given by

$$h_r = 1, \tag{6a}$$

$$h_\theta = r, \tag{6b}$$

$$h_\zeta = 1 + \frac{r}{R}\sin\theta. \tag{6c}$$

The generalization of the method from a toroidal waveguide [18] (approximately a plane curve) with two bendings to a helical waveguide (a space curved waveguide for an arbitrary value of the step's angle of the helix) with two bendings is presented in this paper. The derivation is based on Maxwell's equations for the computation of the EM field and the radiation power density at each point during propagation along a helical waveguide, with a radial dielectric profile. The longitudinal components of the fields are developed into the Fourier-Bessel series. The transverse components of the fields are expressed as a function of the longitudinal components in the Laplace transform domain. Finally, the transverse components of the fields are obtained by using the inverse Laplace transform by the residue method, for an arbitrary value of the step's angle of the helix (δ_p).

The wave equations for the electric and magnetic field components in the inhomogeneous dielectric medium $\epsilon(r)$ are derived for a lossy dielectric media in metallic boundaries of the waveguide. The cross-section of the helical waveguide is shown in Fig. 4(b) for the application of the hollow waveguide, in the region $0 \leq r \leq a + \delta_m$, where δ_m is the thickness of the metallic layer, and d is the thickness of the dielectric layer.

The derivation is given for the lossless case to simplify the mathematical expressions. In a linear lossy medium, the solution is obtained by replacing the permittivity ϵ by $\epsilon_c = \epsilon - j(\sigma/\omega)$ in the solutions for the lossless case, where ϵ_c is the complex dielectric constant, and σ is the conductivity of the medium. The boundary conditions for a lossy medium are given after the derivation. For most

materials, the permeability μ is equal to that of free space ($\mu = \mu_0$). The wave equations for the electric and magnetic field components in the inhomogeneous dielectric medium $\epsilon(r)$ are given by

$$\nabla^2\mathbf{E} + \omega^2\mu\epsilon\mathbf{E} + \nabla\left(\mathbf{E}\cdot\frac{\nabla\epsilon}{\epsilon}\right) = 0, \tag{7a}$$

and

$$\nabla^2\mathbf{H} + \omega^2\mu\epsilon\mathbf{H} + \frac{\nabla\epsilon}{\epsilon}\times(\nabla\times\mathbf{H}) = 0, \tag{7b}$$

respectively. The transverse dielectric profile ($\epsilon(r)$) is defined as $\epsilon_0(1+g(r))$, where ϵ_0 represents the vacuum dielectric constant, and $g(r)$ is its profile function in the waveguide. The normalized transverse derivative of the dielectric profile (g_r) is defined as $(1/\epsilon(r))(\partial\epsilon(r)/\partial r)$.

From the transformation of Equations (3a)–(3c) we can derive the Laplacian of the vector $\mathbf{E}$ (i.e., $\nabla^2\mathbf{E}$), and obtain the wave equations for the electric and magnetic fields in the inhomogeneous dielectric medium. It is necessary to find the values of $\nabla\cdot\mathbf{E}$, $\nabla(\nabla\cdot\mathbf{E})$, $\nabla\times\mathbf{E}$, and $\nabla\times(\nabla\times\mathbf{E})$ in order to obtain the value of $\nabla^2\mathbf{E}$, where $\nabla^2\mathbf{E} = \nabla(\nabla\cdot\mathbf{E}) - \nabla\times(\nabla\times\mathbf{E})$. All these values are dependent on the metric coefficients ((4a)–(4c)).

The ζ component of $\nabla^2\mathbf{E}$ is given by

$$(\nabla^2\mathbf{E})_\zeta = \nabla^2 E_\zeta + \frac{2}{Rh_\zeta^2}\left[\sin\theta\frac{\partial}{\partial\zeta}E_r + \cos\theta\frac{\partial}{\partial\zeta}E_\theta\right] - \frac{1}{R^2h_\zeta^2}E_\zeta, \tag{8}$$

where

$$\begin{aligned}\nabla^2 E_\zeta \;=\; & \frac{\partial^2}{\partial r^2}E_\zeta + \frac{1}{r^2}\frac{\partial^2}{\partial\theta^2}E_\zeta + \frac{1}{r}\frac{\partial}{\partial r}E_\zeta \\ & + \frac{1}{h_\zeta}\left[\frac{\sin\theta}{R}\frac{\partial}{\partial r}E_\zeta + \frac{\cos\theta}{rR}\frac{\partial}{\partial\theta}E_\zeta + \frac{1}{h_\zeta}\frac{\partial^2}{\partial\zeta^2}E_\zeta\right].\end{aligned} \tag{9}$$

The longitudinal components of the wave Equations (7a) and (7b) are obtained by deriving the following terms

$$\left[\nabla\left(\mathbf{E}\cdot\frac{\nabla\epsilon}{\epsilon}\right)\right]_\zeta = \frac{1}{h_\zeta}\frac{\partial}{\partial\zeta}\left[E_r g_r\right], \tag{10}$$

and

$$\left[\frac{\nabla\epsilon}{\epsilon}\times(\nabla\times\mathbf{H})\right]_\zeta = j\omega\epsilon\left[\frac{\nabla\epsilon}{\epsilon}\times\mathbf{E}\right]_\zeta = j\omega\epsilon g_r E_\theta. \tag{11}$$

The longitudinal components of the wave Equations (7a) and (7b) are then written in the form

$$\left(\nabla^2\mathbf{E}\right)_\zeta + k^2 E_\zeta + \frac{1}{h_\zeta}\frac{\partial}{\partial\zeta}\left(E_r g_r\right) = 0, \tag{12}$$

$$\left(\nabla^2\mathbf{H}\right)_\zeta + k^2 H_\zeta + j\omega\epsilon g_r E_\theta = 0, \tag{13}$$

where $(\nabla^2\mathbf{E})_\zeta$, for instance, is given in Equation (8). The *local* wave number parameter is $k = \omega\sqrt{\mu\epsilon(r)} = k_0\sqrt{1+g(r)}$, where the free-space wave number is $k_0 = \omega\sqrt{\mu_0\epsilon_0}$.

The transverse Laplacian operator is defined as

$$\nabla_\perp^2 \equiv \nabla^2 - \frac{1}{h_\zeta^2}\frac{\partial^2}{\partial\zeta^2}. \tag{14}$$

The Laplace transform

$$\tilde{a}(s) = \mathcal{L}\{a(\zeta)\} = \int_{\zeta=0}^{\infty} a(\zeta)e^{-s\zeta}d\zeta \tag{15}$$

is applied on the ζ-dimension, where $a(\zeta)$ represents any ζ-dependent variables, where $\zeta = (R\phi_c)/\cos(\delta_p)$.

The next steps are given in detail in [15, 18], as a part of our derivation. Let us repeat these main steps, in brief.

The longitudinal components of the fields (E_ζ, H_ζ) are developed into Fourier-Bessel series as follows:

$$\tilde{E}_\zeta(s) = \sum_{n'}\sum_{m'}\left[A_{n'm'}(s)\cos(n'\theta) + B_{n'm'}(s)\sin(n'\theta)\right]J_{n'}\left(P_{n'm'}\frac{r}{a}\right), \tag{16a}$$

$$\tilde{H}_\zeta(s) = \sum_{n'}\sum_{m'}\left[C_{n'm'}(s)\cos(n'\theta) + D_{n'm'}(s)\sin(n'\theta)\right]J_{n'}\left(P'_{n'm'}\frac{r}{a}\right), \tag{16b}$$

where P_{nm} and P'_{nm} are the mth roots of the equations $J_n(x) = 0$ and $dJ_n(x)/dx = 0$, respectively.

By substituting Equation (8) into Equation (12) and by using the Laplace transform (15), the longitudinal components of the wave equations (Equations (12) and (13)) are described in the Laplace transform domain, as *coupled* wave equations. The transverse fields for the first section of the helical hollow waveguide with two bendings at $\zeta = \zeta_1$ are obtained directly from the Maxwell equations, and by using the Laplace transform (15). The transverse fields for the first section of the helical hollow waveguide are dependent only on the longitudinal components of the fields and as function of the step's angle (δ_p) of the helix, as follows:

$$\tilde{E}_{r_1}(s) = \frac{1}{s^2+k^2h_{\zeta_1}^2}\left\{-\frac{j\omega\mu_0}{r}\left[\frac{r}{R_1}\cos\theta\cos^2(\delta_p)\tilde{H}_{\zeta_1} + h_{\zeta_1}\frac{\partial}{\partial\theta}\tilde{H}_{\zeta_1}\right]h_{\zeta_1}\right.$$
$$\left. + s\left[\frac{\sin\theta}{R_1}\cos^2(\delta_p)\tilde{E}_{\zeta_1} + h_{\zeta_1}\frac{\partial}{\partial r}\tilde{E}_{\zeta_1}\right] + sE_{r_0} - j\omega\mu_0 H_{\theta_0}h_{\zeta_1}\right\}. \tag{17a}$$

$$\tilde{E}_{\theta_1}(s) = \frac{1}{s^2+k^2h_{\zeta_1}^2}\left\{\frac{s}{r}\left[\frac{r}{R_1}\cos\theta\cos^2(\delta_p)\tilde{E}_{\zeta_1} + h_{\zeta_1}\frac{\partial}{\partial\theta}\tilde{E}_{\zeta_1}\right]\right.$$
$$\left. + j\omega\mu_0 h_{\zeta_1}\left[\frac{\sin\theta}{R_1}\cos^2(\delta_p)\tilde{H}_{\zeta_1} + h_{\zeta_1}\frac{\partial}{\partial r}\tilde{H}_{\zeta_1}\right] + sE_{\theta_0} + j\omega\mu_0 H_{r_0}h_{\zeta_1}\right\}, \tag{17b}$$

$$\tilde{H}_{r_1}(s)=\frac{1}{s^2+k^2h_{\zeta_1}^2}\left\{\frac{j\omega\epsilon}{r}\left[\frac{r}{R_1}\cos\theta\cos^2(\delta_p)\tilde{E}_{\zeta_1}+h_{\zeta_1}\frac{\partial}{\partial\theta}\tilde{E}_{\zeta_1}\right]h_{\zeta_1}\right.$$
$$\left.+s\left[\frac{\sin\theta}{R_1}\cos^2(\delta_p)\tilde{H}_{\zeta_1}+h_{\zeta_1}\frac{\partial}{\partial r}\tilde{H}_{\zeta_1}\right]+sH_{r_0}+j\omega\epsilon E_{\theta_0}h_{\zeta_1}\right\}, \quad (17c)$$

$$\tilde{H}_{\theta_1}(s)=\frac{1}{s^2+k^2h_{\zeta_1}^2}\left\{\frac{s}{r}\left[\frac{r}{R_1}\cos\theta\cos^2(\delta_p)\tilde{H}_{\zeta_1}+h_{\zeta_1}\frac{\partial}{\partial\theta}\tilde{H}_{\zeta_1}\right]\right.$$
$$\left.-j\omega\epsilon h_{\zeta_1}\left[\frac{\sin\theta}{R_1}\cos^2(\delta_p)\tilde{E}_{\zeta_1}+h_{\zeta_1}\frac{\partial}{\partial r}\tilde{E}_{\zeta_1}\right]+sH_{\theta_0}-j\omega\epsilon E_{r_0}h_{\zeta_1}\right\}, \quad (17d)$$

where ζ_1 is the coordinate along the first section of the helical axis, R_1 is the radius of the cylinder of the first section of the helical axis, where the metric coefficient is $h_{\zeta_1}=1+(r/R_1)\sin\theta\cos^2(\delta_p)$. The transverse fields are substituted into the *coupled* wave equations. The longitudinal components of the fields are developed into Fourier-Bessel series, in order to satisfy the metallic boundary conditions of the circular cross-section. The condition is that we have only ideal boundary conditions for $r=a$. Thus, the electric and magnetic fields will be zero in the metal. Two sets of equations are obtained by substitution the longitudinal components of the fields into the wave equations. The first set of the equations is multiplied by $\cos(n\theta)J_n(P_{nm}r/a)$, and after that by $\sin(n\theta)J_n(P_{nm}r/a)$, for $n\neq 0$. Similarly, the second set of the equations is multiplied by $\cos(n\theta)J_n(P'_{nm}r/a)$, and after that by $\sin(n\theta)J_n(P'_{nm}r/a)$, for $n\neq 0$. In order to find an algebraic system of four equations with four unknowns, it is necessary to integrate over the area (r,θ), where $r=[0,a]$, and $\theta=[0,2\pi]$, by using the orthogonal-relations of the trigonometric functions. The propagation constants β_{nm} and β'_{nm} of the TM and TE modes of the hollow waveguide [19] are given, respectively, by $\beta_{nm}=\sqrt{k_o^2-(P_{nm}/a)^2}$ and $\beta'_{nm}=\sqrt{k_o^2-(P'_{nm}/a)^2}$, where the transverse Laplacian operator $(\nabla_\perp^2)$ is given by $-(P_{nm}/a)^2$ and $-(P'_{nm}/a)^2$ for the TM and TE modes of the hollow waveguide, respectively.

2.1. The Elements of the Boundary Conditions' Vectors in the Entrance of the First Section of the Helical Waveguide.

The separation of variables is obtained by using the orthogonal-relations. Thus the algebraic equations ($n\neq 0$) are given by

$$\alpha_n^{(1)}A_n+\beta_n^{(1)}D_n=\frac{1}{\pi}\widehat{(BC1)}_n, \quad (18a)$$

$$\alpha_n^{(2)}B_n+\beta_n^{(2)}C_n=\frac{1}{\pi}\widehat{(BC2)}_n, \quad (18b)$$

$$\beta_n^{(3)} B_n + \alpha_n^{(3)} C_n = \frac{1}{\pi}\widehat{(BC3)}_n, \tag{18c}$$

$$\beta_n^{(4)} A_n + \alpha_n^{(4)} D_n = \frac{1}{\pi}\widehat{(BC4)}_n. \tag{18d}$$

Further we assume $n' = n = 1$. The elements ($\alpha_n^{(1)}$, $\beta_n^{(1)}$, etc), on the left side of (18a) for $n = 1$ are given for an arbitrary value of the step's angle (δ_p) for the first section of the helical waveguide by:

$$\begin{aligned}
\alpha_1^{(1)mm'} = {} & \pi\left(s^2 + \beta_{1m'}^2\right)\left[\left(s^2 + k_0^2\right) G_{00}^{(1)mm'} + k_0^2 G_{01}^{(1)mm'}\right] \\
& + \pi \frac{1}{R_1^4} k_0^2 s^2 \left(\frac{1}{4}\cos^4(\delta_p) G_{02}^{(1)mm'} + \frac{1}{2}\cos^4(\delta_p) G_{03}^{(1)mm'}\right) \\
& + \pi k_0^2 \Bigg\{ s^2 G_{01}^{(1)mm'} + G_{05}^{(1)mm'} + \frac{1}{R_1^2}\left(G_{00}^{(1)mm'} + G_{01}^{(1)mm'}\right) \\
& + \frac{3}{2R_1^2}\beta_{1m'}^2 \cos^4(\delta_p)\left(G_{02}^{(1)mm'} + G_{03}^{(1)mm'}\right) \\
& + \frac{1}{4R_1^4}\cos^4(\delta_p)\left(G_{02}^{(1)mm'} + G_{03}^{(1)mm'}\right) \\
& + \frac{1}{8R_1^4}\cos^8(\delta_p)\left(G_{06}^{(1)mm'} + G_{07}^{(1)mm'}\right)\Bigg\} \\
& + \pi s^2 \Bigg[G_{08}^{(1)mm'} + \frac{1}{2R_1^2}\cos^2(\delta_p) G_{00}^{(1)mm'} \\
& + \frac{1}{4R_1^2}\left(\cos^4(\delta_p)\beta_{1m'}^2 G_{02}^{(1)mm'} + \cos^2(\delta_p) G_{09}^{(1)mm'}\right) \\
& + \frac{1}{2R_1^2}\frac{P_{1m'}}{a}\cos^2(\delta_p)\left(G_{10}^{(1)mm'} + \frac{1}{2}\cos^2(\delta_p) G_{11}^{(1)mm'}\right)\Bigg] \\
& + \pi k_0^4 \cos^4(\delta_p)\Bigg[\frac{3}{2R_1^2}\left(G_{03}^{(1)mm'} + G_{04}^{(1)mm'}\right) \\
& + \frac{1}{8R_1^4}\cos^8(\delta_p)\left(G_{07}^{(1)mm'} + G_{12}^{(1)mm'}\right)\Bigg],
\end{aligned} \tag{19a}$$

$$\begin{aligned}
\beta_1^{(1)mm'} = {} & -j\omega\mu_0\pi s\Bigg\{ G_{13}^{(1)mm'} + \left(\frac{1}{2}\cos^2(\delta_p) + \frac{3}{4}\cos^4(\delta_p)\right)\frac{1}{R_1^2} G_{14}^{(1)mm'} \\
& + \left(\frac{1}{2} + \cos^2(\delta_p)\right)\frac{1}{R_1^2} G_{15}^{(1)mm'} - \frac{1}{2R_1^2} G_{00}^{(1)mm'} \\
& - \cos^2(\delta_p)\frac{1}{R_1^2}\frac{P'_{1m'}}{a} G_{16}^{(1)mm'}\Bigg\},
\end{aligned} \tag{19b}$$

where the elements of the matrices ($G_{00}^{(1)mm'}$, etc.) are given in

Appendix A. Similarly, the rest of the elements on the left side in Equations (18a)–(18d) are obtained. We establish an algebraic system of four equations with four unknowns. All the elements of the matrices in the Laplace transform domain are dependent on the step's angle of the helix (δ_p), the Bessel functions; the dielectric profile $g(r)$; the transverse derivative $g_r(r)$; and (r, θ).

The elements of the boundary conditions' vectors on the right side in Equations (18a)–(18d) are changed at the entrance of every section of the helical waveguide with two bendings. These elements are given in conjunction with the excitation of every section, as follows:

$$\widehat{(BC1)}_1 = \int_0^{2\pi}\int_0^a (BC1)\cos(\theta)J_1(P_{1m}r/a)rdrd\theta, \tag{20a}$$

$$\widehat{(BC2)}_1 = \int_0^{2\pi}\int_0^a (BC2)\sin(\theta)J_1(P_{1m}r/a)rdrd\theta, \tag{20b}$$

$$\widehat{(BC3)}_1 = \int_0^{2\pi}\int_0^a (BC3)\cos(\theta)J_1(P'_{1m}r/a)rdrd\theta, \tag{20c}$$

$$\widehat{(BC4)}_1 = \int_0^{2\pi}\int_0^a (BC4)\sin(\theta)J_1(P'_{1m}r/a)rdrd\theta. \tag{20d}$$

In the case of the TEM_{00} mode in excitation for the first section of the helical waveguide with two bendings (Fig. 1(a)), the elements of the boundary conditions' vectors are obtained, where:

$$\begin{aligned} BC1 = BC2 = {} & j\omega\mu_0 H^+_{\theta_0} s g_r h^2_{\zeta_1} + \frac{2}{R_1}h_{\zeta_1}\sin\theta\left(j\omega\mu_0 H^+_{\theta_0}s + k^2 E^+_{r_0}h_{\zeta_1}\right) \\ & + \frac{2}{R_1}h_{\zeta_1}\cos\theta\left(-j\omega\mu_0 H^+_{r_0}s + k^2 E^+_{\theta_0}h_{\zeta_1}\right) + k^2 h^3_{\zeta_1}E^+_{r_0}g_r, \end{aligned} \tag{21a}$$

$$\begin{aligned} BC3 = BC4 = {} & -j\omega\epsilon E^+_{\theta_0} s g_r h^2_{\zeta_1} + \frac{2}{R_1}h_{\zeta_1}\sin\theta\left(k^2 h_{\zeta_1}H^+_{r_0} - j\omega\epsilon s E^+_{\theta_0}\right) \\ & + \frac{2}{R_1}h_{\zeta_1}\cos\theta\left(k^2 h_{\zeta_1}H^+_{\theta_0} + j\omega\epsilon s E^+_{r_0}\right) + k^2 h^3_{\zeta_1}H^+_{r_0}g_r. \end{aligned} \tag{21b}$$

The elements of the boundary conditions (e.g., $\widehat{(BC2)}_1$) at $\zeta = 0^+$ on the right side in (18b) are given by

$$\begin{aligned} (BC2)_1 = {} & \left[\left(s^2 + k^2 h^2_{\zeta_1}\right)\left(sE_{\zeta_0} + E'_{\zeta_0}\right)\right] + j\omega\mu_0 H_{\theta_0} s g_r h^2_{\zeta_1} \\ & + \frac{2}{R_1}h_{\zeta_1}\sin\theta\left(j\omega\mu_0 H_{\theta_0}s + k^2 E_{r_0}h_{\zeta_1}\right) \\ & + \frac{2}{R_1}h_{\zeta_1}\cos\theta\left(-j\omega\mu_0 H_{r_0}s + k^2 E_{\theta_0}h_{\zeta_1}\right) + k^2 h^3_{\zeta_1}E_{r_0}g_r, \end{aligned}$$

where the metric coefficient is $h_{\zeta_1} = 1 + (r/R_1)\sin\theta\cos^2(\delta_p)$.

The boundary conditions at $\zeta_1 = 0^+$ for TEM_{00} mode in excitation become to

$$\begin{aligned}\widehat{(BC2)}_1 = 2\pi &\left\{\int_0^a Q(r)(k(r)+js)k(r)J_{1m}(P_{1m}r/a)rdr\right\}\delta_{1n} \\ &+\frac{4js\pi}{R_1^2}\cos^2(\delta_p)\left\{\int_0^a Q(r)k(r)J_{1m}(P_{1m}r/a)r^2dr\right\}\delta_{1n} \\ &+\frac{9\pi}{2R_1^2}\cos^4(\delta_p)\left\{\int_0^a Q(r)k^2(r)J_{1m}(P_{1m}r/a)r^3dr\right\}\delta_{1n} \\ &+\frac{3js\pi}{2R_1^2}\cos^4(\delta_p)\left\{\int_0^a Q(r)k(r)J_{1m}(P_{1m}r/a)r^3dr\right\}\delta_{1n} \\ &+\frac{8\pi}{R_1^2}\cos^2(\delta_p)\left\{\int_0^a Q(r)k^2(r)J_{1m}(P_{1m}r/a)r^2dr\right\}\delta_{1n}, \quad (22)\end{aligned}$$

where

$$Q(r) = \frac{E_0}{n_c(r)+1}g_r\exp\left(-(r/w_o)^2\right).$$

Similarly, the remaining elements of the boundary conditions at $\zeta = 0^+$ are obtained. The matrix system of the Equations (18a)–(18d) is solved to obtain the coefficients (A_1, B_1, etc).

According to the Gaussian beams [20] the parameter w_0 is the minimum spot-size at the plane $z = 0$, and the electric field at the plane $z = 0$ is given by $E = E_0\exp[-(r/w_o)^2]$. The modes excited at $\zeta = 0$ in the waveguide by the conventional CO_2 laser IR radiation ($\lambda = 10.6\,\mu$m) are closer to the TEM polarization of the laser radiation. The TEM_{00} mode is the fundamental and most important mode. This means that a cross-section of the beam has a Gaussian intensity distribution. The relation between the electric and magnetic fields [20] is given by $E/H = \sqrt{\mu_0/\epsilon_0} \equiv \eta_0$, where η_0 is the intrinsic wave impedance. Suppose that the electric field is parallel to the y-axis. Thus the components of E_y and H_x are written by the fields $E_y = E_0\exp[-(r/w_o)^2]$ and $H_x = -(E_0/\eta_0)\exp[-(r/w_o)^2]$.

After a Gaussian beam passes through a lens and before it enters to the waveguide, the waist cross-sectional diameter ($2w_0$) can then be calculated approximately for a parallel incident beam by means of $w_0 = \lambda/(\pi\theta) \simeq (f\lambda)/(\pi w)$. This approximation is justified if the parameter w_0 is much larger than the wavelength λ. The parameter of the waist cross-sectional diameter ($2w_0$) is taken into account in our method, instead of the focal length of the lens (f). The initial fields at $\zeta = 0^+$ are formulated by using the Fresnel coefficients of the

transmitted fields [21] as follows

$$E^{+}_{r_0}(r,\theta,\zeta=0^{+}) = T_E(r)(E_0 e^{-(r/w_o)^2}\sin\theta), \tag{23a}$$

$$E^{+}_{\theta_0}(r,\theta,\zeta=0^{+}) = T_E(r)(E_0 e^{-(r/w_o)^2}\cos\theta), \tag{23b}$$

$$H^{+}_{r_0}(r,\theta,\zeta=0^{+}) = -T_H(r)((E_0/\eta_0) e^{-(r/w_o)^2}\cos\theta), \tag{23c}$$

$$H^{+}_{\theta_0}(r,\theta,\zeta=0^{+}) = T_H(r)((E_0/\eta_0) e^{-(r/w_o)^2}\sin\theta), \tag{23d}$$

where $E^{+}_{\zeta_0}(r) = H^{+}_{\zeta_0} = 0$, $T_E(r) = 2/[n(r)+1]$, $T_H(r) = 2n(r)/[n(r)+1]$, and $n(r) = (\epsilon_r(r))^{1/2}$. The index of refraction is denoted by $n(r)$. The index of refraction is denoted by $n(r)$.

2.2. The Transverse Components of the Fields of the First Section of the Helical Waveguide, at $\zeta = \zeta_1$.

The output transverse components of the fields of the helical waveguide are dependent also on the step's angle of the helix (δ_p) and the radius of the cylinder of the helix for the first section (R_1). The output transverse components of the fields are finally expressed in a form of *transfer matrix functions* for the first bending of the helical waveguide as follows:

$$\begin{aligned}
E_{r_1}(r,\theta,\zeta_1) = E^{+}_{r0}(r)e^{-jkh_{\zeta_1}\zeta_1} &- \frac{j\omega\mu_0}{R_1}h_{\zeta_1}\cos^2\theta\cos^2(\delta_p)\sum_{m'} C^{m'}_{S1}(\zeta_1)J_1(\psi) \\
&- \frac{j\omega\mu_0}{R_1}h_{\zeta_1}\sin\theta\cos\theta\cos^2(\delta_p)\sum_{m'} D^{m'}_{S1}(\zeta_1)J_1(\psi) \\
&+ \frac{j\omega\mu_0}{r}h^2_{\zeta_1}\sin\theta\sum_{m'} C^{m'}_{S1}(\zeta_1)J_1(\psi) \\
&- \frac{j\omega\mu_0}{r}h^2_{\zeta_1}\cos\theta\sum_{m'} D^{m'}_{S1}(\zeta_1)J_1(\psi) \\
&+ \frac{1}{R_1}\sin\theta\cos\theta\cos^2(\delta_p)\sum_{m'} A^{m'}_{S2}(\zeta_1)J_1(\xi) \\
&+ \frac{1}{R_1}\sin^2\theta\cos^2(\delta_p)\sum_{m'} B^{m'}_{S2}(\zeta_1)J_1(\xi) \\
&+ h_{\zeta_1}\cos\theta\sum_{m'} A^{m'}_{S2}(\zeta_1)\frac{dJ_1}{dr}(\xi) \\
&+ h_{\zeta_1}\sin\theta\sum_{m'} B^{m'}_{S2}(\zeta_1)\frac{dJ_1}{dr}(\xi),
\end{aligned} \tag{24}$$

where $h_{\zeta_1} = 1 + (r/R_1)\sin\theta\cos^2(\delta_p)$, R is the radius of the cylinder, δ_p is the the step's angle, $\psi = [P'_{1m'}(r/a)]$ and $\xi = [P_{1m'}(r/a)]$. The coefficients are given in the above equation, for instance

$$A_{S1}^{m'}(\zeta_1) = \mathcal{L}^{-1}\left\{\frac{A_{1m'}(s)}{s^2 + k^2(r)h_{\zeta_1}^2}\right\}, \tag{25a}$$

$$A_{S2}^{m'}(\zeta_1) = \mathcal{L}^{-1}\left\{\frac{sA_{1m'}(s)}{s^2 + k^2(r)h_{\zeta_1}^2}\right\}, \tag{25b}$$

where

$$m' = 1, \ldots N, \quad 3 \le N \le 50. \tag{25c}$$

Similarly, the other transverse components of the output fields are obtained. The first fifty roots (zeros) of the equations $J_1(x) = 0$ and $dJ_1(x)/dx = 0$ may be found in tables [22, 23].

2.3. The Elements of the Boundary Conditions' Vectors in the Entrance of the Second Section of the Helical Waveguide at $\zeta = \zeta_1$

The elements of the boundary conditions' vectors (20a)–(20d) in the case of the TEM_{00} mode in excitation for the second section of the helical waveguide with two bendings are obtained from the algebraic system of Equations (18a)–(18d) for $n = 1$, as follows:

$$\begin{aligned} BC1 \;=\; & BC2 = j\omega\mu_0 H_\theta(\zeta = \zeta_1)sg_r h_{\zeta_2}^2 \\ & + \frac{2}{R_2}\sin\theta h_{\zeta_2}\left(j\omega\mu_0 H_\theta(\zeta = \zeta_1)s + k^2 E_r(\zeta = \zeta_1)h_{\zeta_2}\right) \\ & + \frac{2}{R_2}\cos\theta h_{\zeta_2}\left(-j\omega\mu_0 H_r(\zeta = \zeta_1)s + k^2 E_\theta(\zeta = \zeta_1)h_{\zeta_2}\right) \\ & + k^2 h_{\zeta_2}^3 E_r(\zeta = \zeta_1)g_r, \end{aligned} \tag{26a}$$

$$\begin{aligned} BC3 \;=\; & BC4 = -j\omega\epsilon E_\theta(\zeta = \zeta_1)sg_r h_{\zeta_2}^2 \\ & + \frac{2}{R_2}\sin\theta h_{\zeta_2}\left(k^2 h_{\zeta_2} H_r(\zeta = \zeta_1) - j\omega\epsilon s E_\theta(\zeta = \zeta_1)\right) \\ & + \frac{2}{R_2}\cos\theta h_{\zeta_2}\left(k^2 h_{\zeta_2} H_\theta(\zeta = \zeta_1) + j\omega\epsilon s E_r(\zeta = \zeta_1)\right) \\ & + k^2 h_{\zeta_2}^3 H_r(\zeta = \zeta_1)g_r. \end{aligned} \tag{26b}$$

Equations (26a)–(26b) are different from Equations (21a)–(21b) by the initial fields. The initial field, for instance, at the entrance of the first section of the helical waveguide at $\zeta = 0^+$ is denoted as $E_{r_0}^+$

according to (23a), but the initial field of the second section of the helical waveguide in the entrance, at $\zeta = \zeta_1$, is denoted as $E_r(\zeta = \zeta_1)$, according to (24). Similarly, the remaining initial fields are obtained.

These expressions (26a), (26b) are dependent on the radius of the cylinder of the helix of the first section (R_1) and the second section (R_2) of the helical waveguide with two bendings ($R_1 \neq R_2$). Note that these expressions are given also for arbitrary values of the step's angle (and not for small values of the step angles). Actually, these expressions ((26a), (26b)) for the helical waveguide with two bendings consist of all the information at the output fields of the first section (the Bessel-equations, the dielectric profile $g(r)$, the transverse derivative $g_r(r)$, the parameters of the cross-section (r, θ), and the propagation constants β_{nm} and β'_{nm} of the TM and TE modes of the hollow waveguide, respectively).

2.4. The Transverse Fields for the Second Helical Waveguide at $\zeta = \zeta_1 + \zeta_2$

The expression $[1/(s^2 + k^2 h_{\zeta_1}^2)](sE_{r_0}^+ - j\omega\mu_0 H_{\theta_0}^+ h_{\zeta_1})$ in Equation (17a) for the first section of the helical waveguide with two bendings depends on the inital fields $E_{r_0}^+$ (23a) and $H_{\theta_0}^+$ (23d). In the same principle we have the expression $[1/(s^2 + k^2 h_{\zeta_2}^2)](sE_r(\zeta = \zeta_1) - j\omega\mu_0 H_\theta(\zeta = \zeta_1)h_{\zeta_2})$ for the second section of the helical waveguide with two bendings, that depends on the output fields $E_r(\zeta = \zeta_1)$ and $H_\theta(\zeta = \zeta_1)$ (e.g., (24)) at $\zeta = \zeta_1$ of the first section of the helical waveguide with two bendings.

The values of the input fields of the second section of the helical waveguide with two bendings are functions of the parameters of the first section (R_1, ζ_1, and h_{ζ_1}) and the second section (R_2, ζ_2, and h_{ζ_2}) as shown in Fig. 1(a). The expressions are functions of the cross-section (r, θ), the sum of the modes and the old coefficients of the first section of the helical waveguide with two bendings.

The output transverse components of the fields of the helical waveguide are dependent also on the step's angle of the helix (δ_p) and the radius of the cylinder of the helix for the first section (R_1) and for the second section (R_2). The output transverse components of the fields are finally expressed in a form of *transfer matrix functions*

as follows

$$E_r(r,\theta,\zeta=\zeta_1+\zeta_2)=E_{r_0}^{+}e^{-jk(r)(h_{\zeta_1}\zeta_1+h_{\zeta_2}\zeta_2)}$$
$$+\cos(kh_{\zeta_2}\zeta_2)\left(-\frac{j\omega\mu_0}{R_1}h_{\zeta_1}\cos^2\theta\cos^2(\delta_p)\sum_{m'}C_{S1}^{m'}(\zeta_1)J_1(\psi)\right.$$
$$-\frac{j\omega\mu_0}{R_1}h_{\zeta_1}\sin\theta\cos\theta\cos^2(\delta_p)\sum_{m'}D_{S1}^{m'}(\zeta_1)J_1(\psi)+\frac{j\omega\mu_0}{r}h_{\zeta_1}^2\sin\theta\sum_{m'}C_{S1}^{m'}(\zeta_1)J_1(\psi)$$
$$-\frac{j\omega\mu_0}{r}h_{\zeta_1}^2\cos\theta\sum_{m'}D_{S1}^{m'}(\zeta_1)J_1(\psi)+\frac{1}{R_1}\sin\theta\cos\theta\cos^2(\delta_p)\sum_{m'}A_{S2}^{m'}(\zeta_1)J_1(\xi)$$
$$\left.+\frac{1}{R_1}\sin^2\theta\cos^2(\delta_p)\sum_{m'}B_{S2}^{m'}(\zeta_1)J_1(\xi)+h_{\zeta_1}\cos\theta\sum_{m'}A_{S2}^{m'}\frac{dJ_1}{dr}(\xi)+h_{\zeta_1}\sin\theta\sum_{m'}B_{S2}^{m'}\frac{dJ_1}{dr}(\xi)\right)$$
$$-\frac{\sin(kh_{\zeta_2}\zeta_2)}{kh_{\zeta_2}}(j\omega\mu_0h_{\zeta_2})\left(-\frac{j\omega\epsilon}{R_1}h_{\zeta_1}\sin\theta\cos\theta\cos^2(\delta_p)\sum_{m'}A_{S1}^{m'}(\zeta_1)J_1(\xi)\right.$$
$$-\frac{j\omega\epsilon}{R_1}h_{\zeta_1}\sin^2\theta\cos^2(\delta_p)\sum_{m'}B_{S1}^{m'}(\zeta_1)J_1(\xi)-j\omega\epsilon h_{\zeta_1}^2\cos\theta\sum_{m'}A_{S1}^{m'}\frac{dJ_1}{dr}(\xi)$$
$$-j\omega\epsilon h_{\zeta_1}^2\sin\theta\sum_{m'}B_{S1}^{m'}\frac{dJ_1}{dr}(\xi)+\frac{\cos^2\theta}{R_1}\cos^2(\delta_p)\sum_{m'}C_{S2}^{m'}(\zeta_1)J_1(\psi)$$
$$+\frac{1}{R_1}\sin\theta\cos\theta\cos^2(\delta_p)\sum_{m'}D_{S2}^{m'}(\zeta_1)J_1(\psi)-\frac{1}{r}h_{\zeta_1}\sin\theta\sum_{m'}C_{S2}^{m'}(\zeta_1)J_1(\psi)$$
$$\left.+\frac{1}{r}h_{\zeta_1}\cos\theta\sum_{m'}D_{S2}^{m'}(\zeta_1)J_1(\psi)\right)-\frac{j\omega\mu_0}{R_2}h_{\zeta_2}\cos^2\theta\cos^2(\delta_p)\sum_{m'}C_{S1}^{(2)m'}(\zeta_2)J_1(\psi)$$
$$-\frac{j\omega\mu_0}{R_2}h_{\zeta_2}\sin\theta\cos\theta\cos^2(\delta_p)\sum_{m'}D_{S1}^{(2)m'}(\zeta_2)J_1(\psi)$$
$$+\frac{j\omega\mu_0}{r}h_{\zeta_2}^2\sin\theta\sum_{m'}C_{S1}^{(2)m'}(\zeta_2)J_1(\psi)-\frac{j\omega\mu_0}{r}h_{\zeta_2}^2\cos\theta\sum_{m'}D_{S1}^{(2)m'}(\zeta_2)J_1(\psi)$$
$$+\frac{1}{R_2}\sin\theta\cos\theta\cos^2(\delta_p)\sum_{m'}A_{S2}^{(2)m'}(\zeta_2)J_1(\xi)+\frac{1}{R_2}\sin^2\theta\cos^2(\delta_p)\sum_{m'}B_{S2}^{(2)m'}(\zeta_2)J_1(\xi)$$
$$+h_{\zeta_2}\cos\theta\sum_{m'}A_{S2}^{(2)m'}(\zeta_2)\frac{dJ_1}{dr}(\xi)+h_{\zeta_2}\sin\theta\sum_{m'}B_{S2}^{(2)m'}(\zeta_2)\frac{dJ_1}{dr}(\xi),\quad(27)$$

where $\psi=[P'_{1m'}(r/a)]$ and $\xi=[P_{1m'}(r/a)]$, $h_{\zeta_1}=1+(r/R_1)\sin\theta\cos^2(\delta_p)$, and $h_{\zeta_2}=1+(r/R_2)\sin\theta\cos^2(\delta_p)$.

The new coefficients are given in the above equation, for instance

$$A_{S1}^{(2)m'}(\zeta_2) = \mathcal{L}^{-1}\left[\frac{A_{1m'}^{(2)}(s)}{s^2 + k^2(r)h_{\zeta_2}^2}\right], \tag{28a}$$

$$A_{S2}^{(2)m'}(\zeta_2) = \mathcal{L}^{-1}\left[\frac{sA_{1m'}^{(2)}(s)}{s^2 + k^2(r)h_{\zeta_2}^2}\right], \tag{28b}$$

where

$$m' = 1, \ldots N, \quad 3 \leq N \leq 50. \tag{28c}$$

Similarly, the other output transverse components of the fields are obtained, in a form of *transfer matrix functions* (e.g., Equation (27)). The above general solutions of the output transverse components of the fields (e.g., Equation (27)) at $\zeta = \zeta_1 + \zeta_2$ are dependent on the initial fields at $\zeta = \zeta_1$ along the total length $\zeta = \zeta_1 + \zeta_2$, where $\zeta_1 = (R_1\phi_1)/\cos\delta_p$ and $\zeta_2 = (R_2\phi_2)/\cos\delta_p$. Note that the main expression of the solution of the output transverse components of the fields (e.g., Equation (24)) is proportional to $E_{r_0}^{+}\exp[-jk(r)h_{\zeta_1}\zeta_1]$. In the same principle, the main expression for the second section of the helical waveguide with two bendings (e.g., Equation (27)) is proportional to $E_{r_0}^{+}\exp[-jk(r)(h_{\zeta_1}\zeta_1 + h_{\zeta_2}\zeta_2)]$.

These above solutions (e.g., (27)) consist of the sum of the principle expression and other expressions. The principle expression is multiplication of the initial field at $\zeta = 0^+$ (23a) with the exponent $[\exp[-jk(r)(h_{\zeta_1}\zeta_1 + h_{\zeta_2}\zeta_2)]]$. All the above derivation is introduced in the case of the helical waveguide with two bendings in the same direction.

The inverse Laplace transform is performed in this study by a direct numerical integration in the Laplace transform domain by the residue method, as follows

$$f(\zeta) = \mathcal{L}^{-1}[\tilde{f}(s)] = \frac{1}{2\pi j}\int_{\sigma-j_\infty}^{\sigma+j_\infty}\tilde{f}(s)e^{s\zeta}ds = \sum_n \mathrm{Res}[e^{s\zeta}\tilde{f}(s); S_n]. \tag{29}$$

By using the inverse Laplace transform (29) we can compute the output transverse components in the real plane and the output power density at each point at $\zeta = (R\phi_c)/\cos(\delta_p)$. The integration path in the right side of the Laplace transform domain includes all the singularities according to Equation (29). All the points S_n are the poles of $\tilde{f}(s)$ and $\mathrm{Res}[e^{s\zeta}\tilde{f}(s); S_n]$ represent the residue of the function in a specific pole. According to the residue method, two dominant poles for the helical waveguide are given by

$$s = \pm j\ k(r)h_\zeta = \pm j\ k(r)\left(1 + \frac{r}{R}\sin\theta\cos^2(\delta_p)\right).$$

Finally, knowing all the transverse components, the ζ component of the average-power density Poynting vector is given by

$$S_{av} = \frac{1}{2}\mathrm{Re}\left\{E_r H_\theta{}^* - E_\theta H_r{}^*\right\}. \tag{30}$$

where the asterisk indicates the complex conjugate.

The total average-power transmitted along the guide in the ζ direction can be obtained now by the integral of Equation (30) over the waveguide cross section. Thus, the output power transmission is given by

$$T = \frac{1}{2}\int_0^{2\pi}\int_0^a \mathrm{Re}\left\{E_r H_\theta{}^* - E_\theta H_r{}^*\right\} r dr d\theta. \tag{31}$$

Lossy Medium Case

In a linear lossy medium, the solution is obtained by replacing the permittivity ϵ by $\epsilon_c = \epsilon - j(\sigma/\omega)$ in the preceding mathematical expressions, where ϵ_c is the complex dielectric constant and σ is the conductivity of the medium. The coefficients are obtained directly from the algebraic Equations (18a)–(18d) and are expressed as functions in the Laplace transform domain. To satisfy the metallic boundary conditions of a circular cross-section we find the new roots $P_{1m}^{(new)}$ and $P_{1m}^{'(new)}$ of the equations $J_1(z) = 0$ and $dJ_1(z)/dz = 0$, respectively, where z is complex. Thus, from the requirement that the coefficients vanish, the new roots $P_{1m}^{(new)}$ and $P_{1m}^{'(new)}$ are calculated by developing into the Taylor series, in the first order at $1/\sigma$. The new roots in the case of a lossy medium are complex. The complex Bessel functions are computed by using NAG subroutine [24]. The explanation is given in detail in [15].

Several examples computed on a Unix system are presented in the next section, in order to demonstrate the results of this proposed method for the helical waveguide that consists of two bendings. We suppose that the transmitted fields of the initial fields (TEM_{00} mode in excitation) are formulated by using the Fresnel coefficients (23a)–(23d).

3. NUMERICAL RESULTS

This section presents several examples that demonstrate features of the proposed mode model derived in the previous section. The cross-section of the curved waveguide (Fig. 4(b)) is made of a tube of various types of material, a metallic layer, and a dielectric layer upon it. The next examples represent the case of the hollow waveguide with

a metallic layer (Ag) coated by a thin dielectric layer (AgI). For silver having a conductivity of 6.14×10^7 $(\text{ohm} \cdot \text{m})^{-1}$ and the skin depth at 10.6 μm is 1.207×10^{-8} m.

Three test-cases are demonstrated for small values of the step's angle (δ_p). In these cases, $\delta_p \geq 2(a + \delta_m)/(2\pi R)$, according to the condition (2). Note that for small values of the step's angle, the helical waveguide becomes approximately a toroidal waveguide (see Fig. 2), where the radius of the curvature of the helix can then be approximated by the radius of the cylinder (R).

The first test-case is demonstrated for the straight waveguide ($R \to \infty$). The results of the output transverse components of the fields and the output power density ($|S_{av}|$) (e.g., Fig. 5(a)) show the same behavior of the solutions as shown in the results of [15] for the TEM_{00} mode in excitation. The result of the output power density (Fig. 5(a)) is compared also to the result of published experimental data [25] (see also in Fig. 5(b)). This comparison shows good agreement (a Gaussian shape) as expected, except for the secondary small propagation mode. The experimental result (Fig. 5(b)) is affected by the additional parameters (e.g., the roughness of the internal wall of the waveguide) which are not taken theoretically into account. In this example, the length of the straight waveguide is 1 m, the diameter (2a) of the waveguide is 2 mm, the thickness of the dielectric layer $[d_{(AgI)}]$ is 0.75 μm, and the minimum spot-size (w_0) is 0.3 mm. The refractive indices of the air, the dielectric layer (AgI) and the metallic layer (Ag) are $n_{(0)} = 1$, $n_{(AgI)} = 2.2$, and $n_{(Ag)} = 13.5 - j75.3$, respectively. The value of the refractive index of the material at a wavelength of $\lambda = 10.6$ μm is taken from the table compiled by Miyagi et al. in [6].

The second test-case is demonstrated in Fig. 5(c) for the toroidal dielectric waveguide. Fig. 5(d) shows the experimental result that was received in the laboratory of Croitoru at Tel-Aviv University. This experimental result was obtained from the measurements of the transmitted CO_2 laser radiation ($\lambda = 10.6$ μm) propagation through a hollow tube covered on the bore wall with silver and silver-iodide layers (Fig. 4(b)), where the initial diameter (ID) is 1 mm (namely, small bore size).

The output modal profile is greatly affected by the bending, and the theoretical and experimental results (Figs. 5(c)–5(d)) show that in addition to the main propagation mode, several other secondary modes and asymmetric output shape appear. The amplitude of the output power density ($|S_{av}|$) is small as the bending radius (R) is small, and the shape is far from a Gaussian shape. This result agrees with the experimental results, but not for all the propagation modes. The experimental result (Fig. 5(d)) is affected by the bending and

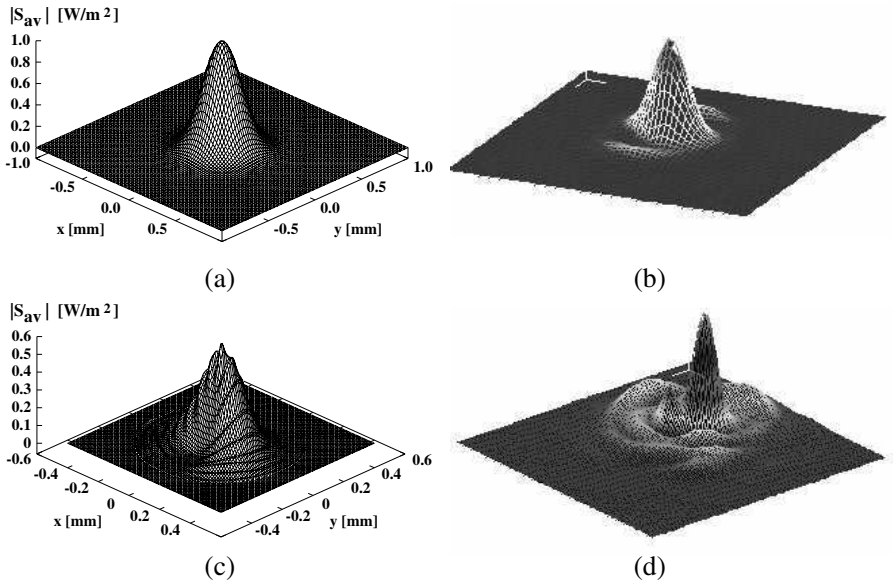

Figure 5. The output power density for $R \to \infty$, where $a = 1\,\text{mm}$, $w_0 = 0.3\,\text{mm}$, and the length of the straight waveguide is 1 m: (a) theoretical result; (b) experimental result. The output power density for the toroidal dielectric waveguide, where $a = 0.5\,\text{mm}$, $w_0 = 0.2\,\text{mm}$, $R = 0.7\,\text{m}$, $\phi = \pi/2$, and $\zeta = 1\,\text{m}$: (c) theoretical result; (d) experimental result. The other parameters are: $d_{(AgI)} = 0.75\,\mu\text{m}$, $\lambda = 10.6\,\mu\text{m}$, $n_{(0)} = 1$, $n_{(AgI)} = 2.2$, and $n_{(Ag)} = 13.5 - j75$.

additional parameters (e.g., the roughness of the internal wall of the waveguide) which are not taken theoretically into account. In this example, $a = 0.5\,\text{mm}$, $R = 0.7\,\text{m}$, $\phi = \pi/2$, and $\zeta = 1\,\text{m}$. The thickness of the dielectric layer $[d_{(AgI)}]$ is $0.75\,\mu\text{m}$ (Fig. 4(b)), and the minimum spot size (w_0) is $0.2\,\text{mm}$. The values of the refractive indices of the air, the dielectric layer (AgI) and the metallic layer (Ag) are $n_{(0)} = 1$, $n_{(AgI)} = 2.2$, and $n_{(Ag)} = 13.5 - j75.3$, respectively. In both theoretical and experimental results (Figs. 5(c)–5(d)) the shapes of the output power density for the curved waveguide are not symmetric.

The third test-case is demonstrated in Fig. 6 for the toroidal waveguide. The theoretical mode-model's result and the experimental result [11] are demonstrated in normalized units where the length of the curved waveguide (ζ) is 0.55 m, the diameter (2a) of the waveguide is 2.4 mm, and the minimum spot size (w_0) is 0.1 mm.

This comparison (Fig. 6) between the theoretical mode-model

and the experimental data [11] shows an approximated result. For all the examples, our theoretical mode-model takes into account only the dielectric losses and the bending losses, in conjunction with the problem of the propagation through a curved waveguide. The experimental result [11] takes into account additional parameters (e.g., the roughness of the internal wall of the waveguide) which are not taken theoretically into account. For small values of the bending $(1/R)$ in the case of small step's angle, the output power transmission is large and decreases with increasing the bending.

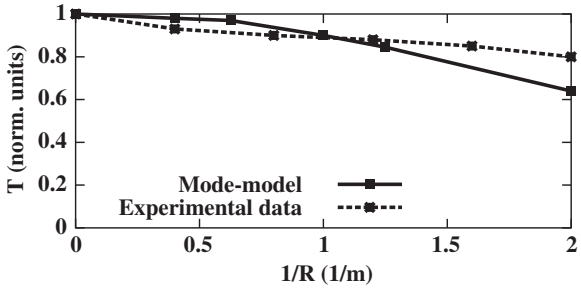

Figure 6. The theoretical mode-model's result and the experimental result [11] where the hollow metallic waveguide (Ag) is covered inside the walls with a AgI film. The output power transmission as a function of $1/R$ for $\delta_p = 0$, where $\zeta = 0.55\,\mathrm{m}$, where $a = 1.2\,\mathrm{mm}$, $d_{(AgI)} = 0.75\,\mu\mathrm{m}$, $w_0 = 0.1\,\mathrm{mm}$, $\lambda = 10.6\,\mu\mathrm{m}$, $n_{(0)} = 1$, $n_{(AgI)} = 2.2$, and $n_{(Ag)} = 10$.

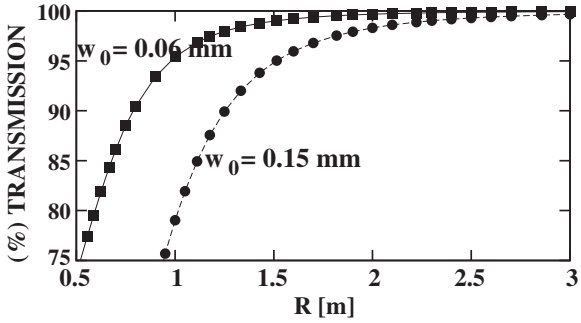

Figure 7. The output power transmission as a function of the radius of the cylinder (R) for $\zeta_1 = 1\,\mathrm{m}$ in two cases of the spot size: (a) $w_0 = 0.06\,\mathrm{mm}$; (b) $w_0 = 0.15\,\mathrm{mm}$, for $\delta_p = 1$. The optimum result is obtained by the first solution of the first section of the helical waveguide.

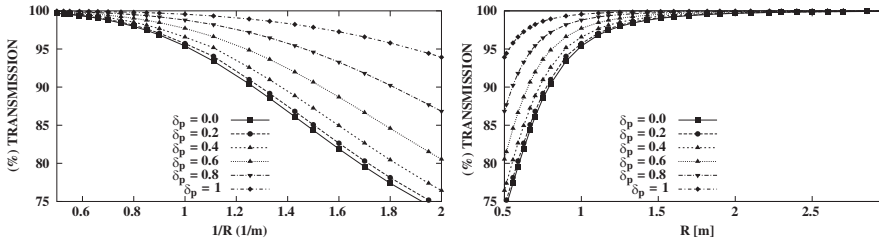

Figure 8. (a) The output power transmission of the helical waveguide as a function of $1/R$, where R is the radius of the cylinder. (b) The output power transmission of the helical waveguide as a function of R. Six results are demonstrated for six values of δ_p ($\delta_p = 0$, 0.2, 0.4, 0.6, 0.8, 1), where $\zeta = 1\,\text{m}$, $a = 1\,\text{mm}$, $w_0 = 0.06\,\text{mm}$, $n_d = 2.2$, and $n_{(Ag)} = 13.5 - j75.3$.

The contribution of this paper is demonstrated in Figs. 7, 8(a), 8(b), 9(a)–9(e) and in Figs. 10(a)–10(e), in order to understand the influence of the step's angle (δ_p) and the radius of the cylinder (R) on the output power transmission, as defined in Equation (31), and the output fields. Fig. 7 represents the effect of the radius of the cylinder on the output power transmission for the first section of the helical waveguide (Fig. 1(a)), for $\delta_p = 1$, where δ_p is the step's angle of the helix. The output power transmission as a function of the radius of the cylinder (R) of the helix is shown in Fig. 7 where the length of the first section of the helical waveguide (ζ_1) is 1 m, and where the values of the spot-size (w_0) are 0.06 mm and 0.15 mm. The diameter (2a) of the waveguide is 2 mm, and the value of the refractive index of the material at a wavelength of $\lambda = 10.6\,\mu\text{m}$. The output power transmission (T) is at least equal to 75% ($75\% \leq T \leq 100\%$). The optimum result is obtained where the spot-size (w_0) is 0.06 mm.

Figure 8(a) demonstrates the influence of the step's angle and the bending ($1/R$) on the output power transmission. Fig. 8(b) demonstrates the influence of the step's angle and the radius of the cylinder (R) on the output power transmission. Figs. 8(a) and 8(b) are demonstrated for six values of δ_p ($\delta_p = 0$, 0.2, 0.4, 0.6, 0.8, 1), where the length of the first section of the helical waveguide (ζ_1) is 1 m, and where the values of the spot-size (w_0) is 0.06 mm. The diameter (2a) of the waveguide is 2 mm, and the value of the refractive index of the material at a wavelength of $\lambda = 10.6\,\mu\text{m}$. The output power transmission (T) is at least equal to 75% ($75\% \leq T \leq 100\%$).

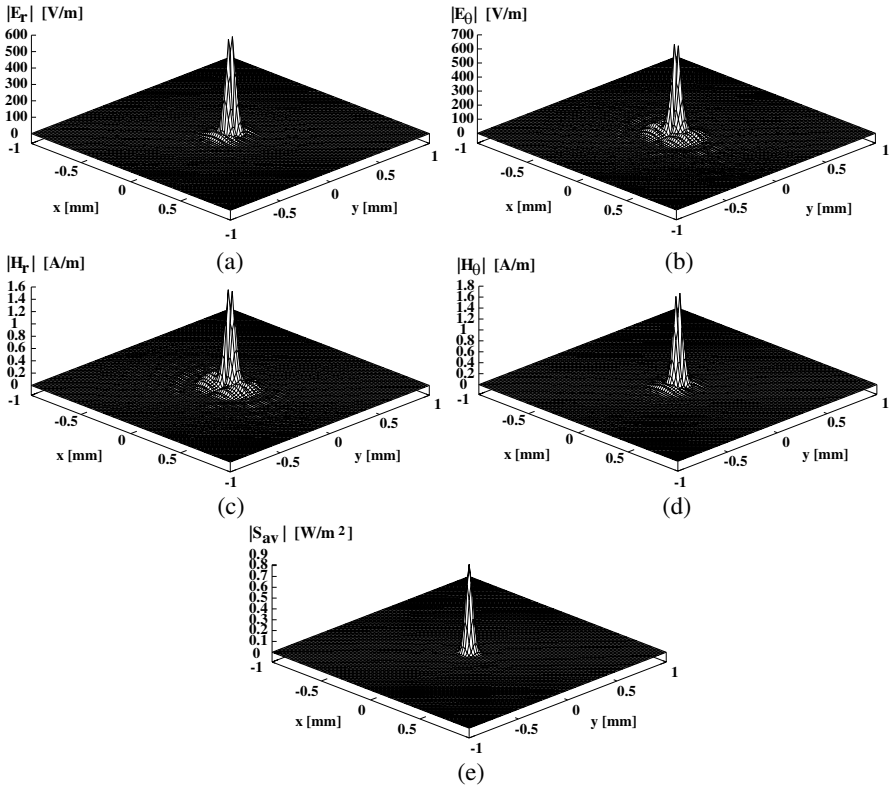

Figure 9. The solution of the output transverse components (a)–(d), and the output power density (e) in the case of the helical waveguide with two bendings, where $\delta_p = 0.5$, $R_1 = 0.5\,\mathrm{m}$ and $R_2 = 0.4\,\mathrm{m}$, $\phi_1 = \pi$, $\phi_2 = \pi/2$, $a = 1\,\mathrm{mm}$, $d_{(AgI)} = 0.75\,\mu\mathrm{m}$, $\lambda = 10.6\,\mu\mathrm{m}$, $w_0 = 0.06\,\mathrm{mm}$, $n_{(0)} = 1$, $n_{(AgI)} = 2.2$, and $n_{(Ag)} = 13.5 - j75.3$.

For an arbitrary value of R, the output power transmission is large for large values of δ_p and decreases with decreasing the value of δ_p. On the other hand, for an arbitrary value of δ_p, the output power transmission is large for large values of R and decreases with decreasing the value of R. Note that for small values of the step's angle, the radius of the curvature of the helix can be approximated by the radius of the cylinder (R). In this case, the output power transmission is large for small values of the bending ($1/R$), and decreases with increasing the bending. Thus, this model can be a useful tool to find the parameters (δ_p and R) which will give us the improved results (output power transmission) of a helical hollow waveguide in the cases of space curved waveguides.

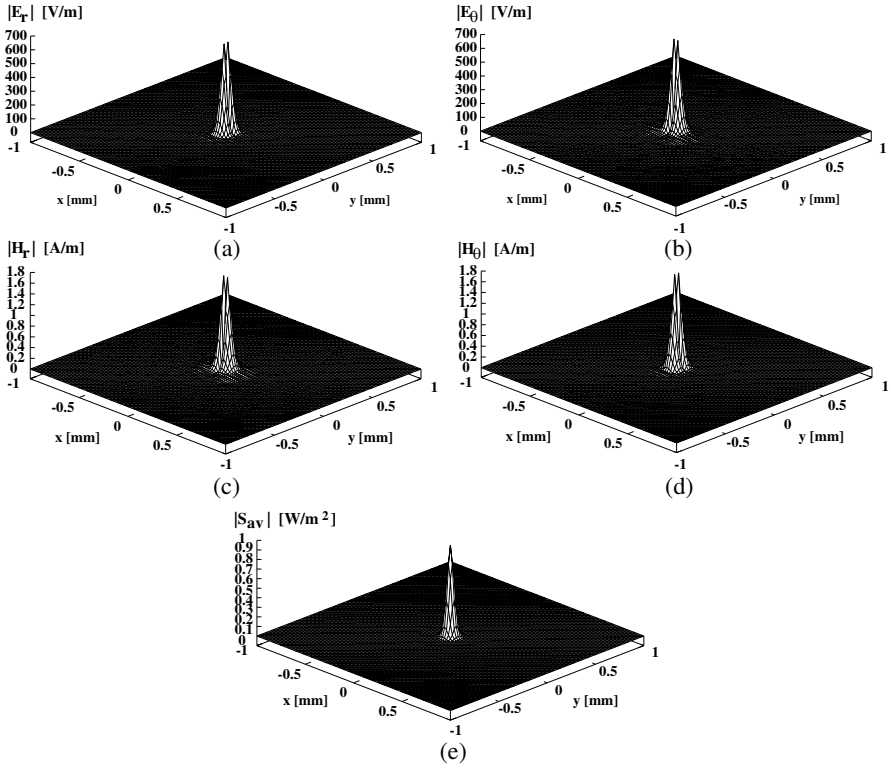

Figure 10. The solution of the output transverse components (a)–(d), and the output power density (e) in the case of the helical waveguide with two bendings, where $\delta_p = 1$, $R_1 = 0.5\,\mathrm{m}$ and $R_2 = 0.4\,\mathrm{m}$, $\phi_1 = \pi$, $\phi_2 = \pi/2$, $a = 1\,\mathrm{mm}$, $d_{(AgI)} = 0.75\,\mu\mathrm{m}$, $\lambda = 10.6\,\mu\mathrm{m}$, $w_0 = 0.06\,\mathrm{mm}$, $n_{(0)} = 1$, $n_{(AgI)} = 2.2$, and $n_{(Ag)} = 13.5 - j75.3$.

Figures 9(a)–9(e) show the results of the output transverse components and the output power density of the field where $\delta_p = 0.5$, $R_1 = 0.5\,\mathrm{m}$ and $R_2 = 0.4\,\mathrm{m}$, $\phi_1 = \pi$, $\phi_2 = \pi/2$, $a = 1\,\mathrm{mm}$, $d_{(AgI)} = 0.75\,\mu\mathrm{m}$, $\lambda = 10.6\,\mu\mathrm{m}$, $w_0 = 0.06\,\mathrm{mm}$, $n_{(0)} = 1$, $n_{(AgI)} = 2.2$, and $n_{(Ag)} = 13.5 - j75.3$. The output transverse components of the field show that in addition to the main propagation mode, several other secondary modes appear.

By increasing only the parameter of the step's angle of the helical waveguide with two bendings ($R_1 = 0.5\,\mathrm{m}$, $R_2 = 0.4\,\mathrm{m}$) from $\delta_p = 0.5$ to $\delta_p = 1$, the results of the output transverse components and the output power density of the field are changed, as shown in Figs. 10(a)–10(e). The amplitude of the output power density in Fig. 9(e) is smaller

as regard to the amplitude of the output power density in Fig. 10(e). The amplitude is small as the step's angle of the helical waveguide is small.

The output results are greatly affected by the step's angle, by the radius of the cylinder of the helix, and by the spot size (w_0). This mode model can be a useful tool in order to determine the optimal conditions for practical applications (output fields, output power density and output power transmission as function of the step's angle and the radius of the cylinder of the helix). This mode model can be a useful tool to improve the output results in all the cases of the helical hollow waveguides with two bendings for industrial and medical regimes.

4. CONCLUSIONS

The main objective was to generalize the method [18] to provide a numerical tool for the calculation of the output transverse fields and the output power density in the case of the helical waveguide that consists of two bendings in the same direction, as shown in Fig. 1(a). The main steps of the method for the helical waveguide with two bendings are given in the derivation, in detail, for an arbitrary value of the step's angle of the helix.

Three test-cases were demonstrated for small values of the step's angle (δ_p). In these cases, $\delta_p \geq 2(a + \delta_m)/(2\pi R)$, according to the condition (2). Note that for small values of the step's angle, the helical waveguide becomes approximately a toroidal waveguide (see Fig. 2), where the radius of the curvature of the helix can then be approximated by the radius of the cylinder (R).

The first test-case was demonstrated for the straight waveguide ($R \to \infty$). The results of the output transverse components of the fields and the output power density ($|S_{av}|$) (e.g., Fig. 5(a)) show the same behavior of the solutions as shown in the results of [15] for the TEM_{00} mode in excitation. The result of the output power density (Fig. 5(a)) was compared also to the result of published experimental data [25] (see also in Fig. 5(b)). This comparison shows good agreement (a Gaussian shape) as expected, except for the secondary small propagation mode. The experimental result (Fig. 5(b)) is affected by the additional parameters (e.g., the roughness of the internal wall of the waveguide) which are not taken theoretically into account.

The second test-case was demonstrated in Fig. 5(c) for the toroidal waveguide, and Fig. 5(d) shows the experimental result. The output modal profile is greatly affected by the bending, and the theoretical and experimental results (Figs. 5(c)–5(d)) show that in addition to the main propagation mode, several other secondary modes and

asymmetric output shape appear. The amplitude of the output power density ($|S_{av}|$) is small as the bending radius (R) is small, and the shape is far from a Gaussian shape. This result agrees with the experimental results, but not for all the propagation modes. The experimental result (Fig. 5(d)) is affected by the bending and additional parameters (e.g., the roughness of the internal wall of the waveguide) which are not taken theoretically into account. In both theoretical and experimental results (Figs. 5(c)–5(d)) the shapes of the output power density for the curved waveguide are not symmetric.

The third test-case was demonstrated in Fig. 6 for the toroidal dielectric waveguide. This comparison (Fig. 6) between the theoretical mode-model and the experimental data [11] shows an approximated result. For all the examples, our theoretical mode-model takes into account only the dielectric losses and the bending losses, in conjunction with the problem of the propagation through a curved waveguide. The experimental result [11] takes into account additional parameters (e.g., the roughness of the internal wall of the waveguide) which are not taken theoretically into account. For small values of the bending ($1/R$) in the case of small step's angle, the output power transmission is large and decreases with increasing the bending.

The contribution of this paper is demonstrated in Figs. 7, 8(a), 8(b), 9(a)–9(e) and in Figs. 10(a)–10(e), in order to understand the influence of the step's angle (δ_p) and the radius of the cylinder (R) on the output power transmission. Fig. 7 represents the effect of the radius of the cylinder on the output power transmission for the first section of the helical waveguide (Fig. 1(a)), for $\delta_p = 1$, where δ_p is the step's angle of the helix. The output power transmission as a function of the radius of the cylinder (R) of the helix is shown in Fig. 7 where the length of the first section of the helical waveguide (ζ_1) is 1 m, and where the values of the spot-size (w_0) are 0.06 mm and 0.15 mm.

Figure 8(a) demonstrates the influence of the step's angle and the bending ($1/R$) on the output power transmission. Fig. 8(b) demonstrates the influence of the step's angle and the radius of the cylinder (R) on the output power transmission. Figs. 8(a) and 8(b) are demonstrated for six values of δ_p (δ_p = 0, 0.2, 0.4, 0.6, 0.8, 1), where the length of the first section of the helical waveguide (ζ_1) is 1 m, and where the values of the spot-size (w_0) is 0.06 mm. In Figs. 7, 8(a), and 8(b), the diameter (2a) of the waveguide is 2 mm, and the value of the refractive index of the material at a wavelength of $\lambda = 10.6\,\mu$m. The output power transmission (T) is at least equal to 75% ($75\% \leq T \leq 100\%$).

For an arbitrary value of R, the output power transmission is large for large values of δ_p and decreases with decreasing the value

of δ_p. On the other hand, for an arbitrary value of δ_p, the output power transmission is large for large values of R and decreases with decreasing the value of R. Note that for small values of the step's angle, the radius of curvature of the helix can be approximated by the radius of the cylinder (R). In this case, the output power transmission is large for small values of the bending ($1/R$), and decreases with increasing the bending. Thus, this model can be a useful tool to find the parameters (δ_p and R) which will give us the improved results (output power transmission) of a helical hollow waveguide in the cases of space curved waveguides.

The output transverse components of the field (Figs. 9(a)–9(d)) show that in addition to the main propagation mode, several other secondary modes appear. The output power density of the field is shown in Fig. 9(e). The output results are greatly affected by the step's angle, by the radius of the cylinder of the helix, and by the spot size (w_0).

By increasing only the parameter of the step's angle of the helical waveguide with two bendings ($R_1 = 0.5\,\mathrm{m}$, $R_2 = 0.4\,\mathrm{m}$) from $\delta_p = 0.5$ to $\delta_p = 1$, the output transverse components and the output power density of the field are changed. The amplitude is small as the step's angle of the helical waveguide is small.

This mode model can be a useful tool in order to determine the optimal conditions for practical applications (output fields, output power density and output power transmission as function of the step's angle and the radius of the cylinder of the helix). This mode model can be a useful tool to improve the output results in all the cases of the helical hollow waveguides with two bendings for industrial and medical regimes.

APPENDIX A.

The elements of the matrices ($G_{00}^{(1)mm'}$, etc.) are given by:

$$G_{00}^{(1)mm'} = \int_0^a J_1\left(P_{1m'}\frac{r}{a}\right) J_1\left(P_{1m}\frac{r}{a}\right) r dr \delta_{1n},$$

$$G_{01}^{(1)mm'} = \int_0^a g(r) J_1\left(P_{1m'}\frac{r}{a}\right) J_1\left(P_{1m}\frac{r}{a}\right) r dr \delta_{1n},$$

$$G_{02}^{(1)mm'} = \int_0^a J_1\left(P_{1m'}\frac{r}{a}\right) J_1\left(P_{1m}\frac{r}{a}\right) r^3 dr \delta_{1n},$$

$$G_{03}^{(1)mm'} = \int_0^a g(r) J_1\left(P_{1m'}\frac{r}{a}\right) J_1\left(P_{1m}\frac{r}{a}\right) r^3 dr \delta_{1n},$$

$$G_{04}^{(1)mm'} = \int_0^a g^2(r) J_1\left(P_{1m'}\frac{r}{a}\right) J_1\left(P_{1m}\frac{r}{a}\right) r^3 dr\delta_{1n},$$

$$G_{05}^{(1)mm'} = \int_0^a k^2 g(r) J_1\left(P_{1m'}\frac{r}{a}\right) J_1\left(P_{1m}\frac{r}{a}\right) r dr\delta_{1n},$$

$$G_{06}^{(1)mm'} = \int_0^a J_1\left(P_{1m'}\frac{r}{a}\right) J_1\left(P_{1m}\frac{r}{a}\right) r^5 dr\delta_{1n},$$

$$G_{07}^{(1)mm'} = \int_0^a g(r) J_1\left(P_{1m'}\frac{r}{a}\right) J_1\left(P_{1m}\frac{r}{a}\right) r^5 dr\delta_{1n},$$

$$G_{08}^{(1)mm'} = \int_0^a g_r\left(\frac{P_{1m'}}{a}\right) {J_1}'\left(P_{1m'}\frac{r}{a}\right) J_1\left(P_{1m}\frac{r}{a}\right) r dr,$$

$$G_{09}^{(1)mm'} = \int_0^a g_r J_1\left(P_{1m'}\frac{r}{a}\right) J_1\left(P_{1m}\frac{r}{a}\right) r^2 dr\delta_{1n},$$

$$G_{10}^{(1)mm'} = \int_0^a {J_1}'\left(\frac{P_{1m'}r}{a}\right) J_1\left(P_{1m}\frac{r}{a}\right) r^2 dr\delta_{1n},$$

$$G_{11}^{(1)mm'} = \int_0^a g_r {J_1}'\left(\frac{P_{1m'}r}{a}\right) J_1\left(P_{1m}\frac{r}{a}\right) r^3 dr\delta_{1n},$$

$$G_{12}^{(1)mm'} = \int_0^a g^2(r) J_1\left(P_{1m'}\frac{r}{a}\right) J_1\left(P_{1m}\frac{r}{a}\right) r^5 dr\delta_{1n},$$

$$G_{13}^{(1)mm'} = \int_0^a g_r {J_1}'\left(\frac{p'_{1m'}r}{a}\right) J_1\left(P_{1m}\frac{r}{a}\right) dr\delta_{1n},$$

$$G_{14}^{(1)mm'} = \int_0^a g_r J_1\left(\frac{p'_{1m'}r}{a}\right) J_1\left(P_{1m}\frac{r}{a}\right) r^2 dr\delta_{1n},$$

$$G_{15}^{(1)mm'} = \int_0^a J_1\left(P'_{1m'}\frac{r}{a}\right) J_1\left(P_{1m}\frac{r}{a}\right) r dr\delta_{1n},$$

$$G_{16}^{(1)mm'} = \int_0^a {J_1}'\left(\frac{P'_{1m'}r}{a}\right) J_1\left(P_{1m}\frac{r}{a}\right) r^2 dr\delta_{1n}.$$

Similarly, the remaining elements are obtained. The coefficients are obtained directly from the algebraic system of equations (18a)–(18d) and are expressed as functions in s-plane. Similarly, the other coefficients are obtained.

REFERENCES

1. Harrington, J. A. and Y. Matsuura, "Review of hollow waveguide technology," *SPIE*, Vol. 2396, 1995
2. Harrington, J. A., D. M. Harris, and A. Katzir (eds.), *Biomedical Optoelectronic Instrumentation*, 4–14, 1995.

3. Harrington, J. A., "A review of IR transmitting, hollow waveguides," *Fiber and Integrated Optics*, Vol. 19, 211–228, 2000.
4. Marcatili, E. A. J. and R. A. Schmeltzer, "Hollow metallic and dielectric waveguides for long distance optical transmission and lasers," *Bell Syst. Tech. J.*, Vol. 43, 1783–1809, 1964.
5. Marhic, M. E., "Mode-coupling analysis of bending losses in IR metallic waveguides," *Appl. Opt.*, Vol. 20, 3436–3441, 1981.
6. Miyagi, M., K. Harada, and S. Kawakami, "Wave propagation and attenuation in the general class of circular hollow waveguides with uniform curvature," *IEEE Trans. Microwave Theory Tech.*, Vol. 32, 513–521, 1984.
7. Croitoru, N., E. Goldenberg, D. Mendlovic, S. Ruschin, and N. Shamir, "Infrared chalcogenide tube waveguides," *SPIE*, Vol. 618, 140–145, 1986.
8. Melloni, A., F. Carniel, R. Costa, and M. Martinelli, "Determination of bend mode characteristics in dielectric waveguides," *J. Lightwave Technol.*, Vol. 19, 571–577, 2001.
9. Bienstman, P., M. Roelens, M. Vanwolleghem, and R. Baets, "Calculation of bending losses in dielectric waveguides using eigenmode expansion and perfectly matched layers," *IEEE Photon. Technol. Lett.*, Vol. 14, 164–166, 2002.
10. Mendlovic, D., E. Goldenberg, S. Ruschin, J. Dror, and N. Croitoru, "Ray model for transmission of metallic-dielectric hollow bent cylindrical waveguides," *Appl. Opt.*, Vol. 28, 708–712, 1989.
11. Morhaim, O., D. Mendlovic, I. Gannot, J. Dror, and N. Croitoru, "Ray model for transmission of infrared radiation through multibent cylindrical waveguides," *Opt. Eng.*, Vol. 30, 1886–1891, 1991.
12. Kark, K. W., "Perturbation analysis of electromagnetic eigenmodes in toroidal waveguides," *IEEE Trans. Microwave Theory Tech.*, Vol. 39, 631–637, 1991.
13. Lewin, L., D. C. Chang, and E. F. Kuester, *Electromagnetic Waves and Curved Structures*, Chap. 6, 58–68, Peter Peregrinus Ltd., London, 1977.
14. Menachem, Z., "Wave propagation in a curved waveguide with arbitrary dielectric transverse profiles," *Journal of Electromagnetic Waves and Applications*, Vol. 17, No. 10, 1423–1424, 2003, and *Progress In Electromagnetics Research*, Vol. 42, 173–192, 2003.
15. Menachem, Z., N. Croitoru, and J. Aboudi, "Improved mode model for infrared wave propagation in a toroidal dielectric

waveguide and applications," *Opt. Eng.*, Vol. 41, 2169–2180, 2002.

16. Menachem, Z. and M. Mond, "Infrared wave propagation in a helical waveguide with inhomogeneous cross section and applications," *Progress In Electromagnetics Research,* Vol. 61, 159–192, 2006.
17. Menachem, Z. and M. Haridim, "Propagation in a helical waveguide with inhomogeneous dielectric profiles in rectangular cross section," *Progress In Electromagnetics Research B*, Vol. 16, 155–188, 2009.
18. Menachem, Z., "Flexible hollow waveguide with two bendings for small values of step angles, and applications," *Progress In Electromagnetics Research B,* Vol. 21, 347–383, 2010.
19. Collin, R. E., *Foundation for Microwave Engineering*, McGraw-Hill, New York, 1996.
20. Yariv, A., *Optical Electronics*, 3rd edition, Holt-Saunders Int. Editions, 1985.
21. Baden Fuller, A. J., *Microwaves*, Chap. 5, 118–120, Pergamon Press, A. Wheaton and Co. Ltd, Oxford, 1969.
22. Olver, F. W. J., *Royal Society Mathematical Tables, Zeros and Associated Values*, 2–30, University Press Cambridge, 1960.
23. Jahnke, E. and F. Emde, *Tables of Functions with Formulae and Curves*, Chap. 8, 166, Dover Publications, New York, 1945.
24. The Numerical Algorithms Group (NAG) Ltd., Wilkinson House, Oxford, U.K..
25. Croitoru, N., A. Inberg, M. Oksman, and M. Ben-David, "Hollow silica, metal and plastic waveguides for hard tissue medical applications," *SPIE*, Vol. 2977, 30–35, 1997.